Rheol Acta (2003) 42: 372–382
DOI 10.1007/s00397-002-0286-3

ORIGINAL CONTRIBUTION

D.C.-H. Cheng

Characterisation of thixotropy revisited

Received: 26 December 2000
Accepted: 30 October 2002
Published online: 14 January 2003

D.C.-H. Cheng
Icknield Way, 191, Letchworth,
Herts, SG6 4TT, United Kingdom
E-mail: DCHCheng@aol.com

Abstract This paper re-examines the 'proof' of Cheng and Evans (1965) that the equilibrium flow curve of a thixotropic fluid has a positive slope, and shows that the slope can indeed be negative in parts. The implication of this on thixotropic behaviour in viscometers is described. Such thixotropic fluids can develop shear banding in wide-gap viscometers in common with many other materials, a brief survey of which is given. Additionally, the interrelationship of the Cross and Sisko fluids as models of thixotropy is examined, leading to the creation of a new class of thixotropic models.

Keywords Thixotropy · Cheng-Evans phenomenological theory · Model flow curves · Non-monotonic flow curves · Rheometry · Shear banding · Cross model · Sisko model · New class of thixotropic model

Introduction

In the 1965 paper on the phenomenological characterisation of inelastic thixotropic fluids, Cheng and Evans (1965) showed that the equilibrium flow curve (EFC) has a positive slope along the entire length. However, increasing volume of experimental observation, such as those on metal alloy slurries (Kirkwood 1994; McClelland et al. 1997), which are suspensions of particles in a molten medium, show that steady shear stress can decrease with increasing shear rate. The data can be fitted by the power law model but with a negative n value of −0.3; alternatively, they may be fitted by the Sisko viscosity model with $m = 1.3$. It can be readily shown that the Cross model (Cross 1965; Barnes et al. 1989) (which, although originally developed to describe the flow curve of polymeric solutions, applies just as well to thixotropy) gives an S-shaped steady-shear flow curve under certain conditions when the index m is greater than 1. Other examples of materials, both actual and models showing such non-monotonic flow curves, are given below. All these experimental and theoretical results mean that the conclusion that the EFC has positive slope only has to be re-examined and this is done in this paper. It is shown that the slope can indeed be negative in part.

The significance of this in the description of thixotropic behaviour and in viscometric measurement is described. It is shown that such thixotropic fluids can develop shear banding in wide-gap viscometers. This is in common with many other materials, a brief survey of which is given, and the significance discussed.

Example of flow curves showing negative slope are illustrated by the Cross and Sisko models. The Sisko model (Sisko 1958; Barnes et al. 1989) can be considered to be the high shear rate asymptote of the Cross model, but it has been used to describe experimental results at low shear rates (McLelland et al. 1997; Barnes et al. 1989). The possibility of the Sisko model being a fluid in its own right and applicable down to zero shear rate is considered. This requires the re-examination of the Cross model as a thixotropic fluid, which is not generally appreciated. This is done in this paper. It is shown that the Sisko model does have a separate existence because of a recovery mechanism that is different from the Cross.

This leads to the creation of a new set of thixotropic models.

Slope of the equilibrium flow curve

The constitutive equation for a general inelastic thixotropic fluid is composed of an equation of state and a rate equation (Cheng and Evans 1965):

$$F = \eta(\lambda, D)D \tag{1}$$

$$\frac{d\lambda}{dt} = g(\lambda, D) \tag{2}$$

where F is the shear stress, D shear rate, λ the structural parameter and t time; η is viscosity and g is the rate function when expressed in terms of D. The functional forms of η and g are subject to certain restrictions. Two that are needed below are

$$\left(\frac{\partial F}{\partial D}\right)_{\lambda} > 0 \left(\frac{\partial 9}{\partial D}\right)_{\lambda} < 0 \tag{3}$$

The justification of the first inequality has been given by Cheng and Evans (1965). The second inequality defines thixotropic behaviour. For negative or anti-thixotropy, $(\partial g/\partial D)_{\lambda} > 0$.

Under steady state shearing, $g = g_e = 0$. Equation (2) then gives the equilibrium structure $\lambda_e = \lambda_e(D)$. Substituting this into Eq. (1) gives the equilibrium flow curve (EFC), $F_e = F(\lambda_e, D) = F_e(D)$. The slope of the EFC is $(dF/dD)_e$. The subscript e denotes equilibrium conditions.

In order to determine the sign of the slope, we need first to establish certain inequalities. Expanding the rate equation by the Taylor series about equilibrium and keeping to constant D:

$$g = \left(\frac{\partial g}{\partial \lambda}\right)_c \{\lambda - \lambda_c\} \tag{4}$$

For a thixotropic fluid, we expect that when a structure is more built up than the equilibrium, $\lambda > \lambda_e$ it would undergo breakdown at constant D, i.e. $g < 0$, and vice versa. This requires that

$$\left(\frac{\partial g}{\partial \lambda}\right)_e < 0 \tag{5}$$

The rate equation can equally well be expressed in terms of F by eliminating D between $g(\lambda, D)$ and Eq. (1):

$$\frac{d\lambda}{dt} = f(\lambda, F) = g(\lambda, D) \tag{6}$$

where $f = f(\lambda, F)$ is the rate function expressed in terms of F. Differentiating f and g at constant λ gives

$$\left(\frac{\partial f}{\partial F}\right)_{\lambda} = \left(\frac{\partial g}{\partial D}\right)_{\lambda} \left(\frac{\partial D}{\partial F}\right)_{\lambda} < 0 \tag{7}$$

The inequality follows from Eq. (3). The relationship applies along the EFC at every point.

The last inequality we need concerns $(\partial f/\partial \lambda)_e$. In the previous paper, it was taken that the differential is negative. However, it is now realised that it can in fact take either sign and be positive also, as will be made clear presently.

The slope of the EFC is

$$\left(\frac{dF}{dD}\right)_e = \left(\frac{dF}{\partial \lambda}\right)_e \left(\frac{\partial \lambda}{dD}\right)_e \tag{8}$$

Differentiating g and applying the result at equilibrium, we find that

$$\left(\frac{\partial \lambda}{\partial D}\right)_e = -\left(\frac{\partial g}{\partial D}\right)_e \Big/ \left(\frac{\partial g}{\partial \lambda}\right)_e < 0 \tag{9}$$

The inequality follows from Eqs (3) and (5).

Similarly, from differentiating f and applying the result at equilibrium:

$$\left(\frac{\partial F}{\partial \lambda}\right)_e = -\left(\frac{\partial f}{\partial \lambda}\right)_e \Big/ \left(\frac{\partial f}{\partial F}\right)_e \tag{10}$$

Now $(\partial f/\partial F)_e < 0$ (Eq. 7). If $(\partial f/\partial \lambda)_e$ is negative, then $(\partial F/\partial \lambda)_e$ is negative, and taken with Eq. (8), $(dF/dD)_e$ would be positive. If, on the other hand $(\partial f/\partial \lambda)_e$ is positive, then $(dF/dD)_e$ would be negative and the EFC would have a negative slope. It was supposed by Cheng and Evans (1965) that $(\partial f/\partial \lambda)_e$ is negative and it was concluded that the EFC has a positive slope. However, as outlined in the introduction, this is not the case. This discussion identifies the misconception which led to the earlier incomplete conclusion. It is now clear that the EFC can show a negative slope. The significance of this is discussed further in the next section.

The Cross model is used to illustrate the general argument above. The constitutive equations for the model are

$$F = (\eta_\infty + c\lambda)D \tag{11A}$$

$$g = a(1 - \lambda) - b\lambda D^m \tag{11B}$$

where $c = (\eta_o - \eta_\infty)$. The behaviour of the model is explored with a spreadsheet.

The EFC is

$$F_e = \left(\eta_\infty + \frac{c}{1 + kD^m}\right)D \tag{12}$$

where $k = b/a$. It is plotted in Fig. 1 for the parameters $\eta_o = 0.3$, 5 and 2000 Pa.s; $\eta_\infty = 0.05$ Pa.s, $\kappa = ac/b = 100$ Pa.s$^{1\text{-}m}$ and a range of values of m. The values of η_∞, κ and $m = 1.3$ correspond to certain samples of metal

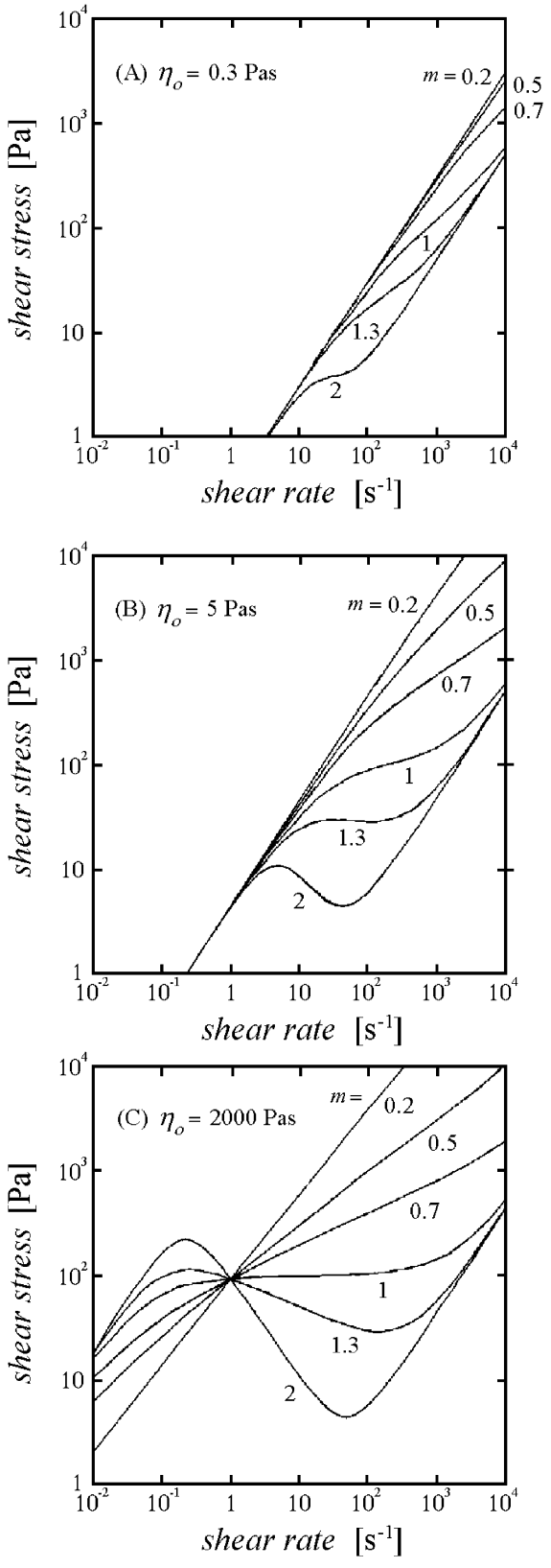

◄

Fig. 1A–C Equilibrium flow curve for Cross model with: **A** $\eta_o = 0.3$ Pa.s; **B** $\eta_o = 5$ Pa.s; **C** $\eta_o = 2000$ Pa.s; $\eta_\infty = 0.05$ Pa.s, $\kappa = ac/b = 100$ Pa.s^{1-m} and a range of values of m

alloy slurries (McLelland et al. 1997). The slope of the EFC is positive for very low and very high shear rates, but it can be negative over a range of medium shear rates. This is determined by the values of c and m. When $m \leq 1$, it is shown below that the slope is positive along the whole length of the flow curve irrespective of c; but when $m > 1$, it can become negative if c is sufficiently large. In Fig 1A for small c ($\eta_o = 0.3$ Pa.s), the slope is positive even when $m = 2$. For a medium value of c ($\eta_o = 5$ Pa.s), it remains positive for m up to nearly 1.3 (Fig. 1B). When c is large, negative slope develops for values of $m > 1$ (Fig. 1C). As $c \to \infty$, the limiting value of m for positive slope is 1.

The shape of the EFC depends on the sign of the differential $(dF/d\lambda)_e$, i.e. the slope of the equilibrium (F_e,λ) curve. This can be easily derived for the Casson model:

$$F_e = (\eta_\infty + c\lambda)\left(\frac{a(1-\lambda)}{b\lambda}\right)^{(1/m)} \tag{13}$$

The spreadsheet is used to plot Fig. 2. Figure 2A illustrates that, for small c, the slope of (F_e,λ) is negative along the whole length even when $m = 2$, corresponding to the positive slope of the EFC in Fig. 1A. For medium c, $m = 1$ gives negative slope still, but when $m = 1.3$ there is a small positive slope round about $\lambda = 0.1$ (just apparent in Fig. 2B), giving the corresponding EFC in Fig. 1B. Figure 2C illustrates the behaviour when c is large. When $m > 1$, namely $m = 1.3$, there is a distinct section of positive slope to the (F_e,λ) curve. The curve for $m = 1$ shows the limiting nature of that value of m. These are reflected in the EFC curves in Fig. 1C.

The slope of the EFC is finally traced to the sign of the differential $(\partial f/\partial\lambda)_e$ of the rate equation. For the Cross model

$$\left(\frac{\partial f}{\partial \lambda}\right) = -a - b\left(\frac{f}{\eta_\infty + c\lambda}\right)^m \left(\frac{\eta_\infty + (1-m)c\lambda}{\eta_\infty + c\lambda}\right) \tag{14}$$

The value at equilibrium $(\partial f/\partial\lambda)_e$ is obtained by substituting corresponding equilibrium values $(F_e(\lambda),\lambda)$ into the equation. It can be seen at once that for $m \leq 1$, the differential is negative irrespective of the value of c and so the EFC has positive slope along the whole length. The spreadsheet is used to explore the behaviour when $m > 1$. Figure 3 (calculated for $a = 1$) illustrates the results for low, medium and high values of c. The range of λ over which the differential is positive (and giving negative slope for the EFC) is clearly shown.

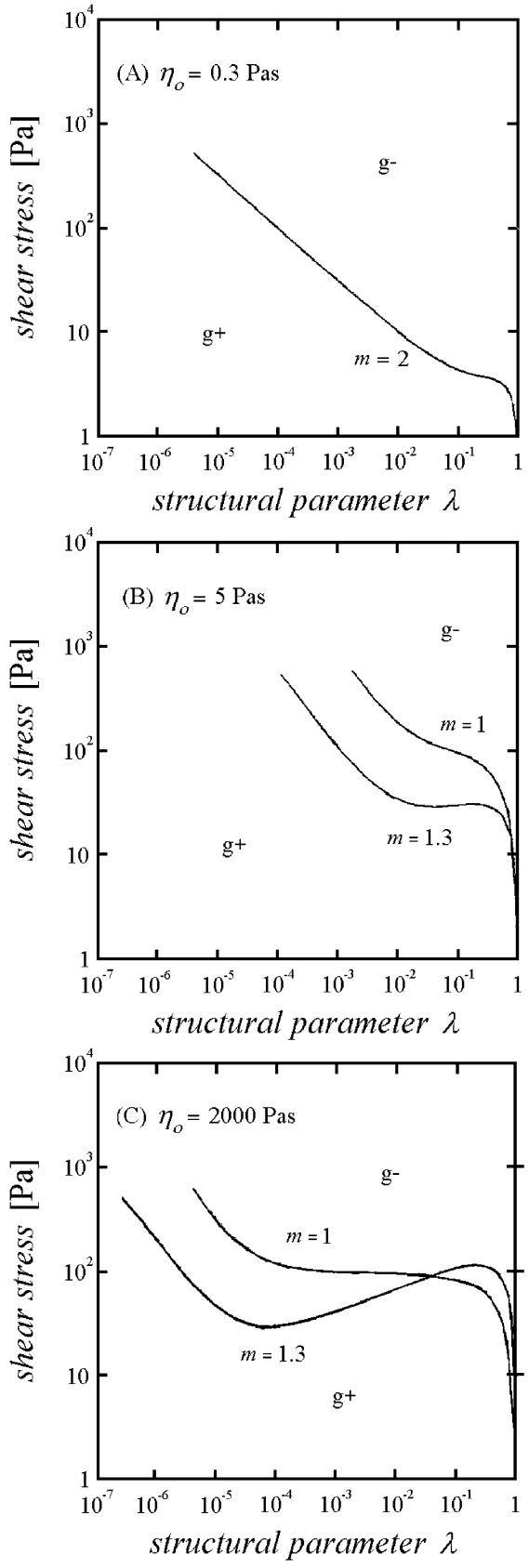

◀

Fig. 2A–C Equilibrium shear stress vs λ for: **A** $\eta_o = 0.3$ Pa.s; **B** $\eta_o = 5$ Pa.s; **C** $\eta_o = 2000$ Pa.s; $\eta_\infty = 0.05$ Pa.s, $\kappa = ac/b = 100$ Pa.s^{1-m} and various values of m

The corresponding range of F is seen in Fig. 2, which in turn is seen in the EFC in Fig. 1.

The negative slope of the EFC can be explained qualitatively in terms of the rate of structural break-down. The break-down is fast when m is large, and this leads to a large decrease of the equilibrium λ_e as shear rate is increased. Together with a large value of c, this makes for a rapid decrease in equilibrium viscosity, and hence shear stress with shear rate. This is not compensated by the increase in shear stress due to the increase in shear rate, and so results in a dramatic decrease in F and the negative slope of the EFC. This continues until the structure is nearly fully broken down, the asymptotic high shear viscosity η_∞ is approached and the flow curve resumes the upward going trend due to the increase in shear stress with shear rate.

Significance of EFC having negative slope

The significance of the EFC having a negative slope in viscometric testing is shown in Fig. 4. To put it into context, the behaviour of an EFC with positive slope is described first (Fig. 5). Thixotropic fluids are tested in viscometers under either constant shear rate or constant shear stress, in the so-called controlled rate (CR) or controlled stress (CS) rheometers respectively. Near a section of the EFC having positive slope (Fig. 5), the structure would change in such a way that it tends towards the equilibrium E. For example, A is being tested at constant D; having $\lambda_3 > \lambda_e(D)$, it is located in the region of negative g (g−) and would break down and move towards E by shear stress decreasing. C, with $\lambda_1 < \lambda_e(F)$, is being tested under constant F; it is in the region of positive f (in which g is also positive, g+) and would move towards E by shear rate decreasing. Similarly for B and G.

Near a section of the EFC with negative slope, the same occurs with testing under constant shear rate (Fig. 4). A′ has $\lambda_3 > \lambda_e(D)$ and g− is negative; the structure undergoes breakdown and moves towards E′. Analogously, B′ also moves towards E′. The behaviour is governed by Eq. (4) and there is nothing unusual about this.

However, for tests under constant shear stress, a different behaviour is found. C′, despite $\lambda_1 < \lambda_e(F)$, is located in the region of negative g− (same as f) and instead of the structure increasing towards the equilibrium E′, $\lambda_e(F)$, it suffers further breakdown. In other words, C′ actually moves away from E′. The same is found with G′: $\lambda_3 > \lambda_e(F)$, but it is located in the region of positive g+; there is further build up and it also

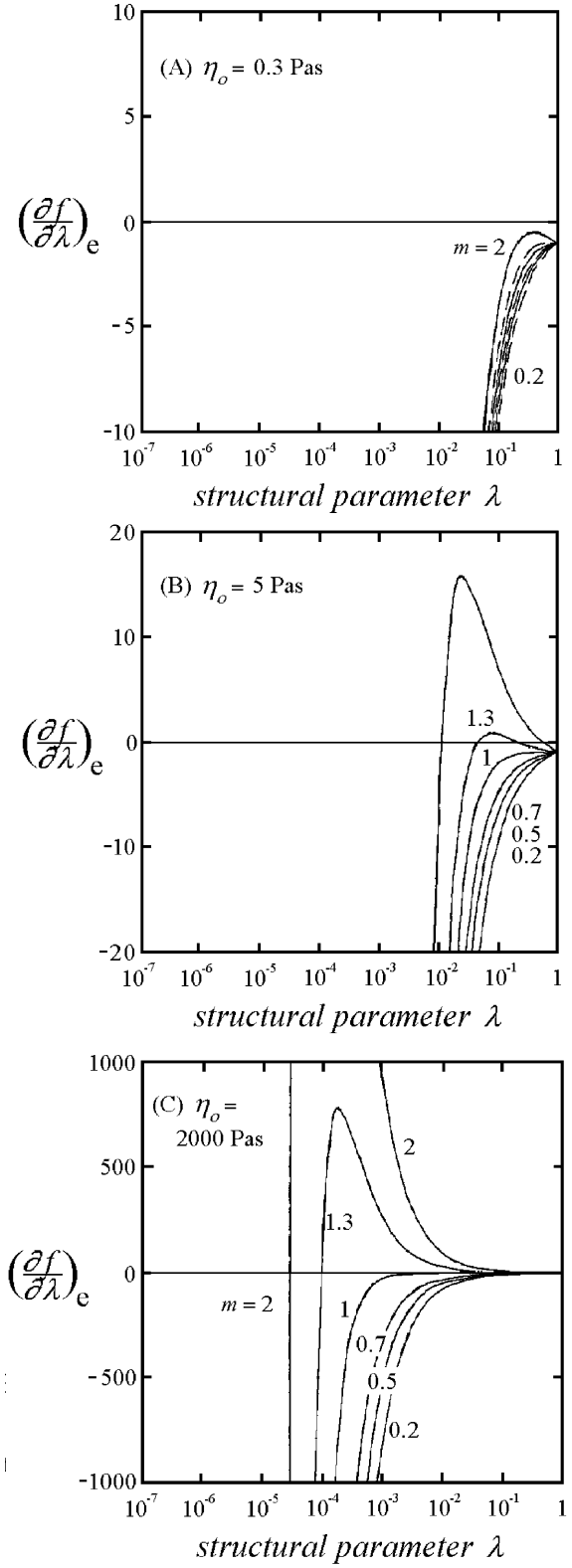

Fig. 3A–C Plot of $(\partial f/\partial\lambda)_e$ vs λ for: **A** $\eta_o = 0.3$ Pa.s; **B** $\eta_o = 5$ Pa.s; **C** $\eta_o = 2000$ Pa.s; $\eta_\infty = 0.05$ Pa.s, $\kappa = ac/b = 100$ Pa.s^{1-m} and a range of values of m; a = 1

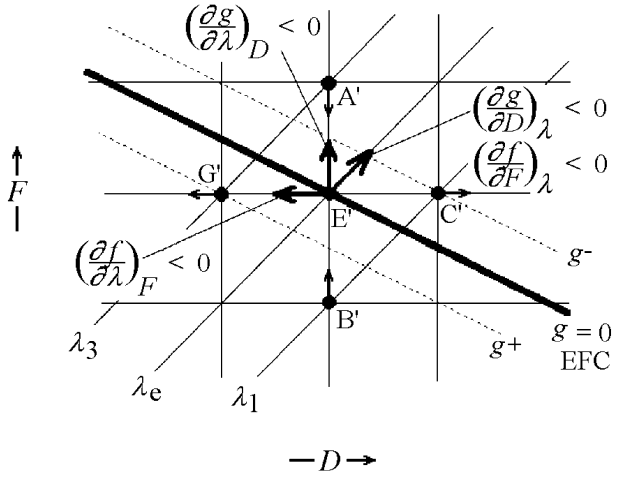

Fig. 4 Structural behaviour close to an equilibrium flow curve with negative slope

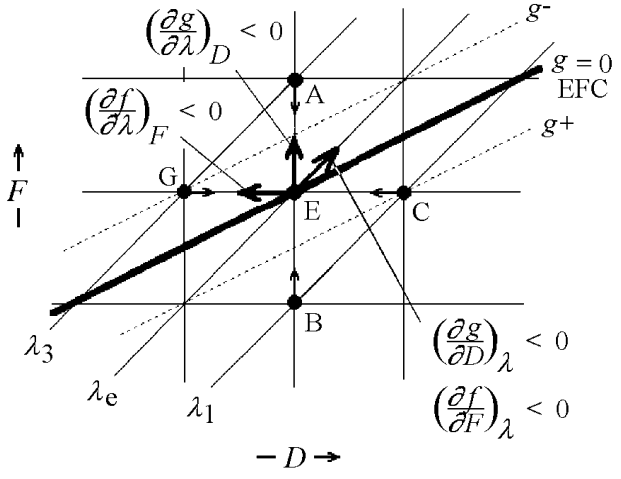

Fig. 5 Structural behaviour close to an equilibrium flow curve with positive slope

moves away from E′. This behaviour is described by an equation analogous to Eq. (4):

$$\frac{d\lambda}{dt} = f = \left(\frac{\partial f}{\partial \lambda}\right)_e \{\lambda - \lambda_e(F)\} \tag{15}$$

If $(\partial f/\partial\lambda)_e$ is negative, the usual behaviour that the structure would tend towards equilibrium E is obtained; this is found when the EFC has a positive slope (Fig. 5). However, if $(\partial f/\partial\lambda)_e$ is positive, a structure $\lambda_3 > \lambda_e(F)$ would continue to increase, and vice versa, under constant shear stress. This is associated with the EFC having a negative slope (Fig. 4). The behaviour is quite contrary to our usual notion of thixotropic behaviour in relation to the equilibrium state, but everything is quite adequately accounted for in mathematical terms.

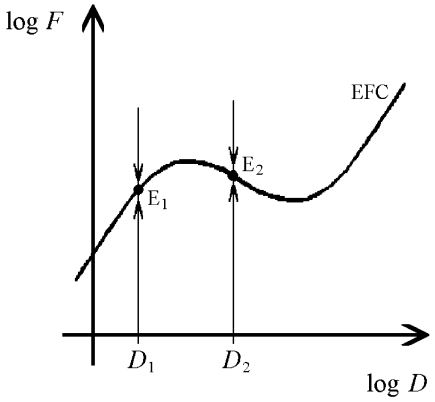

Fig. 6 Approach to equilibrium in tests at constant shear rate

Behaviour in *ideal* CR and CS rheometers

The practical significance of the above is that, while the entirety of the S-shaped EFC is determinable in CR rheometers operating under constant shear rate (Fig. 6), the negatively sloped section is not accessible under constant shear stress testing in CS rheometers. In Fig. 7, carrying out a cycle of stepped shear stresses and maintaining each until equilibrium is reached would trace out (abcef) on the up-sweep and (fedba) for the down-sweep, giving hysteresis behaviour.

The region marked out by (bcedb) can be *probed*, for example, by shearing first at a high shear stress F′ to point H and then suddenly reducing the stress to F″. If the structure along the constant-λ curve (HI) is such that I lies on the left of the EFC, then as F″ is held constant, the sample would move towards the equilibrium point at J. If the shearing at F′ is continued to K before changing to F″, the point L may well fall to the right of the EFC. Then the sample would tend towards the equilibrium at M instead.

In other words, for a shear stress lying between the maximum and minimum, c and d, of the S-shaped EFC,

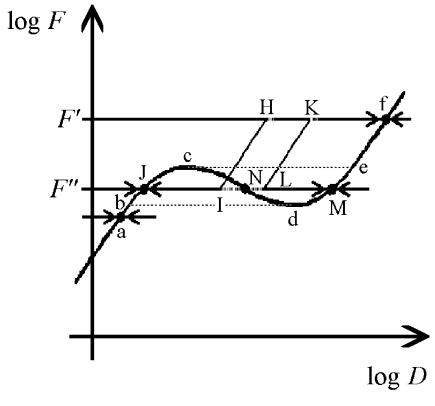

Fig. 7 Approach to equilibrium in tests at constant shear stress

there are three equilibrium points J, M and N. All three are stable equilibrium points under constant shear rate testing. However, under constant shear stress testing only two of them J and M are stable. N is an unstable equilibrium point and cannot be maintained in a CS test and so cannot be accessed.

In the *ideal* CS and CR testing just described, the entire sample is subjected to constant shear stress or shear rate. This can only be performed in a *perfect* parallel plate simple shear instrument. In the usual rheometers, such as the tube or rotational, the shear stress and shear rate are not uniform across the sample. The behaviour of the sample needs more detailed consideration.

CS testing in a wide-gap coaxial cylinder rheometer

The CS testing is the simpler to analyse. Consider as an example the use of a wide gap coaxial cylinder rheometer to determine the EFC. The CS condition can be readily obtained by applying a constant torque T/h per unit length of the cylinder, giving a shear stress distribution $F = (T/2\pi h)/r^2$. The wall shear stresses are F_1 and F_2 on the inner and outer cylinder of radius r_1 and r_2. As long as F_1 is less than F_c the maximum shear stress on the EFC ($F_c = F_e$, Fig. 7), the equilibrium condition is governed by the ...abc portion of the EFC. The condition is conventional and there is no problem in interpreting the experimental speed-torque (Ω,T) curve to determine shear rate.

From equilibrium shearing when $F_1 = F_c$, consider that F_1 is suddenly increased to F_f and held constant. Assuming a wide gap rheometer, the outer cylinder shear stress $F_2 = (r_2/r_1)^2 F_1$ would be very low, say F_a. The shear stress distribution would span $F_a < \{F_c = F_e\} < F_f$. The shear stress at each radial position would be constant and the CS testing behaviour described above would apply. On shearing to equilibrium, the condition for $F < F_c$ would be given by the EFC portion ...abc, while the condition for $F > F_e$ would be given by the portion ef....

The interesting thing to note is that, while the shear stress distribution is monotonic, the shear rate and structure distributions show discontinuities at the radius where $F = F_c = F_e$. There is no velocity discontinuity, only that the local shear rate is bi-valued depending on the direction of approach. This discontinuity in structure and shear rate clearly gives rise to shear banding. The phenomenon is well known with other materials but has not been observed for thixotropic fluids. This is discussed below under Significance and shear banding.

The rotational speed in the coaxial cylinder rheometer is given by the standard result in the literature (Whorlow 1992):

$$\Omega = \frac{1}{2}\int_{F_2}^{F_1} D\frac{dF}{F} = \frac{1}{2}\left(\int_{F_2}^{F_e} D\frac{dF}{F} + \int_{F_e}^{F_1} D\frac{dF}{F}\right) \tag{16}$$

The shear rate at the cylinder D_1 is obtained by differentiating the expression with respect to F_1. Depending on the detailed mathematics, different 'explicit formulae' are obtained. (They have been collected together by Cheng 1980.) As the EFC is sufficiently differentiable at both a and f, and $F_c = F_e$ is constant, there is no problem in the inversion. The conventional expressions for calculating shear rate, the various explicit formulae, apply. This is stated without detailed proof. It is expected that the discontinuity described by ce would be reflected by a discontinuity in slope in the torque-speed curve.

In CS testing when the applied torque and shear stress are reduced, the latter from F_f or higher, it is clear that equilibrium is governed by the portions ...fed and ba... of the EFC. There is no need to go over the details here.

The interpretation of experimental measurements to determine the constant structure curve and breakdown rate in a wide gap rheometer, in which the structure is not uniform, has been studied previously (Cheng and Evans 1965). How the negatively sloped flow curve affect the interpretation is not considered in the present paper.

CR testing in a tube rheometer

Consider now CR testing. It is of course impossible in practice to maintain uniform shear rate in a rheometer. What one actually does is to impose a constant volumetric flow rate in the tube or hold the rotational speed constant. The shear rate is therefore a floating variable which is determined by the sample property and the testing condition. The behaviour of CR testing is therefore somewhat complicated.

For example, consider again the determination of the EFC but in a tube rheometer of radius R (Fig. 8). Suppose that the flow rate Q has been increased until, at equilibrium, the wall condition is given by point c, and then it is increased by a step increase ΔQ. We imagine a numerical simulation by finite difference calculations.

Before the change

$$Q = \pi\int_0^R r^3 D^e(r)dr \tag{17}$$

where the equilibrium shear rate $D^e(r)$ is prescribed by the EFC portion 0abc. (Equation 17 is derived by manipulation of standard result in the literature (Whorlow 1992)). The associated shear stress distribution and wall shear stress are

$$F^e(r) = \left(\frac{r}{2}\right)\left(\frac{P}{L}\right) \quad F_w^e = \left(\frac{R}{2}\right)\left(\frac{P}{L}\right)$$
$$\frac{F^e(r)}{F_w^e} = \frac{r}{R} \tag{18}$$

where P/L is the pressure drop per unit length. The equilibrium structure is distributed accordingly: $\lambda^e(r)$. These values apply at the step change, time $t = 0$, and are considered to be the initial conditions after the step change: $D(r,0)$, $F(r,0) = (r/2)(P/L)$, $F_w(0) = (R/2)(P/L)$ and $\lambda(r,0)$.

On making the step change in flow rate, the shear rate and stress distributions are also changed by $\Delta D(r,0)$ and $\Delta F(r,0)$; $\Delta F_w(0)$. These quantities are determined by the sample property given by the constitutive equations repeated here:

$$D = D(F,\lambda)$$
$$\frac{d\lambda}{dt} = f(\lambda,F) \tag{19}$$

The increases in flow rate and shear rate are related by

$$\Delta Q = \pi\int_0^R r^3\Delta D(r,0)dr \tag{20}$$

while the increase in shear stress is

$$\Delta F(r,0) = \left(\frac{r}{2}\right)\left(\frac{\Delta P}{L}\right) \quad \Delta F_w(0) = \left(\frac{R}{2}\right)\left(\frac{\Delta P}{L}\right)$$
$$\frac{\Delta F(r,0)}{\Delta F_w(0)} - \frac{r}{R} \tag{21}$$

where ΔP is the increase in pressure accompanying the step increase in flow rate. The equilibrium conditions along 0abc, $\lambda^e(r)$, are related to the initial conditions at $t = 0$, 0a′b′c′, $\lambda(r,0)$, by the constant-$\lambda(r,0)$ curves shown in Fig. 8. Along each constant-λ curve, $\Delta\lambda = 0$. Thus, differentiating Eq. (19):

$$\Delta D(r,0) = D_{,F}\,\Delta F(r,0) \tag{22}$$

where $D_{,F} = (\partial D/\partial F)_\lambda$ depends on the local conditions and hence varies with r. At the wall, where $\Delta D(R,0) = \Delta D_w(0)$ and $\Delta F(R,0) = \Delta F_w(0)$:

$$\Delta D_w(0) = (D_{,F})_w\Delta F_w(0) \tag{23}$$

Thus

$$\frac{\Delta D(r,0)}{\Delta D_w(0)} = \frac{D_{,F}}{(D_{,F})_w}\frac{\Delta F(r,0)}{\Delta F_w(0)} = \frac{D_{,F}}{(D_{,F})_w}\frac{r}{R} \tag{24}$$

Substituting into Eq. (20):

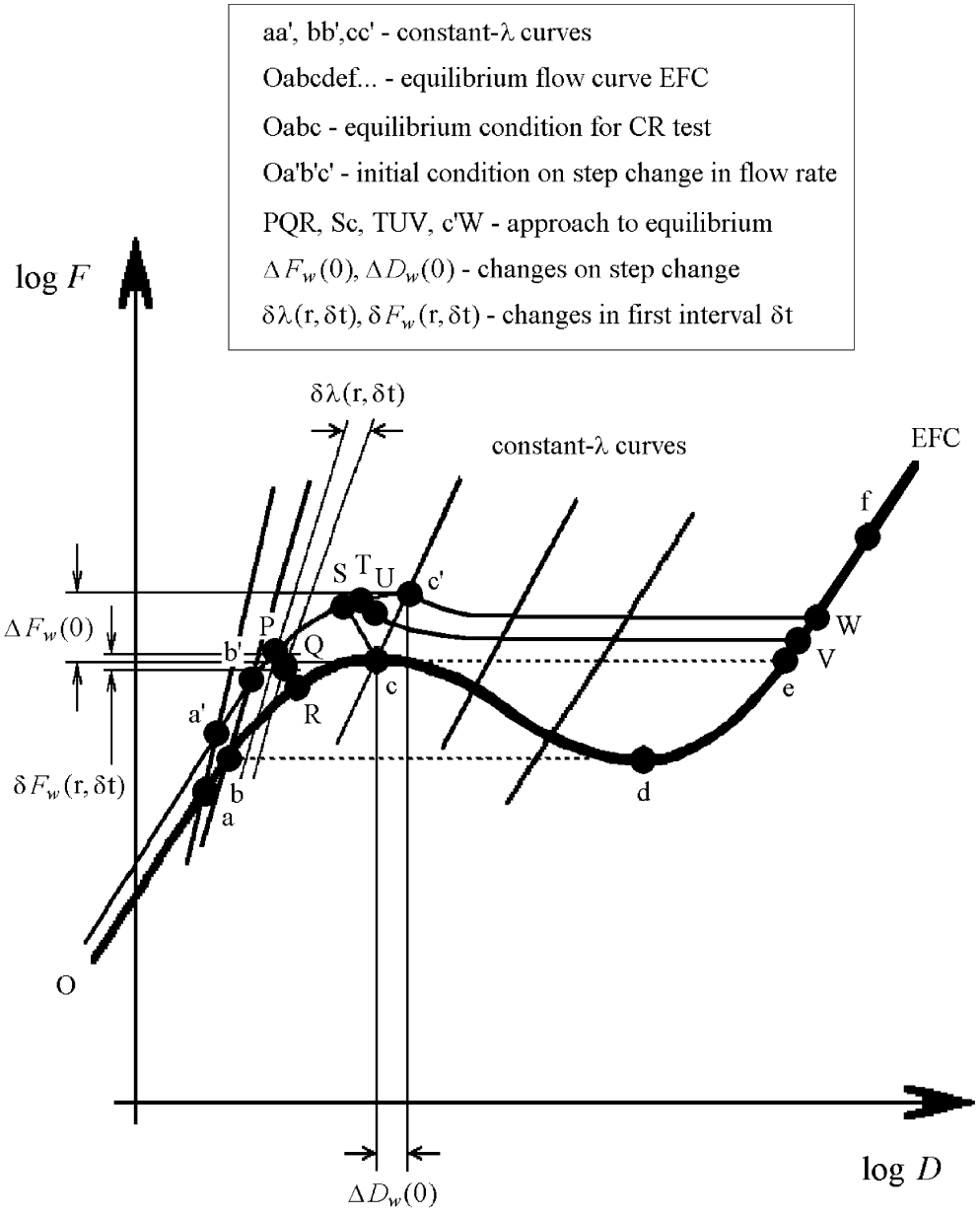

Fig. 8 Approach to equilibrium in tests at constant flow rate in tube rheometer

$$\Delta Q = \left(\frac{\pi}{R(D_{,F})_w}\int_0^R r^4 D_{,F}\, dr\right)\Delta D_w(0) \tag{25}$$

This allows $\Delta D_w(0)$ to be calculated and hence $\Delta F_w(0)$, $\Delta F(r,0)$ and $\Delta D(r,0)$ by using Eqs. (21) and (24) in turn. $D_{,F} = (\partial D/\partial F)_\lambda$ and the wall values $(D_{,F})_w$ are evaluated at the local $F(r,0)$ and $\lambda(r,0)$.

With the initial conditions along 0a′b′c′ thus fixed, the changes with time can then be calculated. The next calculation is to predict the time evolution after the step change.

Over the first time interval δt, the structure undergoes a breakdown given by Eq. (19):

$$\delta\lambda(r,\delta t) = f[\lambda(r,0), F(r,0)]\delta t \tag{26}$$

Next, there is a change in shear stress. Remembering that the CR test is carried out under a constant flow rate of $Q+\Delta Q$, $d\Delta Q/dt = 0$, then from Eq. (20), for a small time interval δt after the step change:

$$0 = \pi\int_0^R r^3 \delta\Delta D(r,0)dr \tag{27}$$

From Eq. (19) and using Eq. (21):

$$\delta D(r,\delta t) = D_{,F}\frac{r}{R}\delta F_w(\delta t) + D_{,\lambda} f(\lambda(r,0), F(r,0))\delta t \tag{28}$$

where $D_{,\lambda} = (\partial D/\partial\lambda)_F$ varies with r. Substituting in Eq. (27) and rearranging:

$$\delta F_w(\delta t) = -\frac{\int_b^R r^3 D_{,\lambda} f[\lambda(r,0), F(r,0)]dr}{\frac{1}{R}\int_0^R r^4 D_{,F}\, dr} \tag{29}$$

With δF_w thus calculated, the change in the shear stress distribution is derived from Eq. (21):

$$\delta F(r, \delta t) = \frac{r}{R}\delta F_w(\delta t) \tag{30}$$

and similarly the shear rate from Eqs. (22) and (23):

$$\begin{aligned} \delta D(r, \delta t) &= D_{,F}\frac{r}{R}\delta F_w(\delta t) \\ \delta D_w(\delta t) &= (D_{,F})_w \delta F_w(\delta t) \end{aligned} \tag{31}$$

By repeating the calculation for further intervals of time, the evolution of structure Eq. (26), shear stress Eqs. (29) and (30) and shear rate Eq. (31) may be followed quantitatively. The exact behaviour depends on the model constitutive equations Eq. (19) assumed.

The approach to equilibrium and the equilibrium conditions can be deduced qualitatively. In Fig. 8, the initial state of the sample at r on step change in speed is, say, P. After the first time interval, the new position, given by $\delta\lambda(r,\delta t)$ and $\delta F(r,\delta t)$, can readily be marked out as Q. As time goes on, the locus of Q heads towards the EFC and would reach it at R at equilibrium. The closer it gets to the tube wall, the higher up would Q be on 0abc. At one particular radius, represented by S on 0a′b′c′, the equilibrium condition would actually be c.

At radius $r_T > r_S$, but close to S, the initial shear stress $F_T(r_T,0)$ would be slightly greater than $F_S(r_S,0)$. As time goes on, U would head towards cd, the portion of the EFC having negative slope. But, the shear stress $F(r_T,t)$ cannot be less than $F(r_S,t)$ and, at equilibrium, $F(r_T,\infty)$ cannot be less than $F(r_S,\infty) = F_c$. It can easily be seen that U would head towards ef... and would end up close to e, at V where $F(r_T,\infty) = F_V$ is just a little greater than $F_e = F_c$. The samples represented by S^+Tc' on 0a′b′c′ therefore end up as eVW on ef....

This condition is the same as that encountered in the CS test described above (Fig. 7). In contrast with the *constant-shear rate* test (Fig. 6), the negatively sloped portion of the EFC is not measured by the *constant-flow rate* test (Fig. 8). There is a discontinuity in the shear rate distribution at some radius, where a discontinuity in structure also exists, giving the shear banding phenomenon as in the CR test. More on shear banding is given in the next section.

For the derivation of the EFC from the experimental measurement, the standard starting equation applies (Whorlow 1992). For conditions where $F_w > F_c = F_e$, it now reads

$$Q = \frac{\pi R^3}{F_w^3}\left(\int_0^{F_c} F^2 D^c(F)dF + \int_{F_c}^{F_w} F^2 D^c(F)dF\right) \tag{32}$$

The shear rate at the tube wall D_w is obtained by differentiating the expression with respect to F_w (Whorlow 1992). As the EFC is sufficiently differentiable above e, and $F_c = F_e$ is constant, there is no problem in the inversion. The conventional expression for calculating shear rate, the well known Mooney-Rabinowitsch equation, applies. This is again stated without detailed proof. It is expected that the discontinuity represented by ce would be reflected by a discontinuity in slope in the pressure drop-flow rate curve.

Similar remarks may be made about the interpretation of CR testing when the flow rate is reduced as has been made above for the coaxial cylinder case when shear stress is reduced.

Significance and shear banding

We can expect that there would be some very interesting and curious behaviour to be found in and around the region bcedb in Fig. 7, when more complicated testing, such as repeated cyclic shearing, is carried out even in the *ideal* rheometer. The exact behaviour can be predicted in detail if a theoretical model is assumed. In practice, thixotropic measurement is not usually carried out using CS rheometers. The result of the present discussion suggests that it would be very informative to do so.

For wide-gap rheometers and the tube, the previous two sections show that shear banding can occur in thixotropic fluids. The shear banding phenomenon is widely described in the literature for many materials, actual and models, that show steady shear flow curve that is non-monotonic and S-shaped: that is, having low and high shear rate arms of positive slope but with a negatively-sloped middle section. Depending on the method of measurement, the flow curve can show up as a constant shear stress plateau or the shear stress, on attaining a maximum value, decreases when the shear rate is further increased. The materials include the metal alloy slurries mentioned in the introduction to this paper, and polymeric systems (Goveas and Fredrickson 1999; Kumar and Larson 2000; Lu, Olmstead and Ball 2000; Olmsted et al. 2000; Remmelgas and Leal 2000; Tanaka 2000), micellar solutions (Bautista et al. 2000; Britton et al. 1999; Decruppe et al. 2000; Eiser et al. 2000; Kumar and Larson 2000; Lee et al. 2000; Lerouge et al. 1998; Radulescu et al. 1999, 2000), liquid crystals (Ferreiro et al. 2000; Radulescu et al. 1999), soils and granular materials (Anand and Gu 2000; Knight 1997; Lu, Zhang and Yang 2000; Oda and Kazama 1998),

other particulate suspensions (Bair and Winer 2000; Volkova et al. 1999), and thermoviscoplastic material (Chen and Batra 1999; Kim and Im 2000).

Theoretical model constitutive equations have been developed for some of these materials. The material structural state is sensitive to shear and this leads to non-monotonic steady shear behaviour and gives rise to shear banding in which the sample in the viscometric gap falls into two distinct bands having different structures and flowing with greatly different low and high shear rates.

It is outside the scope of the present paper to widen the discussion on non-monotonic flow curves and shear banding. However, clearly the mechanism responsible varies from material to material. The thixotropic model discussed here constitutes yet another different structural 'mechanism' for the behaviour. The phenomenological study of thixotropy has gone out of favour in rheological research in recent years while rheologists concentrate more on probing the microrheological nature of specific materials. This explains why the non-monotonic flow curve and the associated shear-banding phenomenon have not hitherto been described in thixotropy.

Relationship between the Cross and Sisko models

The Sisko model flow curve

$$F = \left(\eta_\infty + \frac{K}{D^m}\right)D \tag{33}$$

was originally proposed empirically to describe the viscosity of lubricating greases (Sisko 1958). It has been fitted to certain metal alloys showing negative slope in the EFC (Kirkwood 1994). The model can be considered to be the high shear rate asymptote of the Cross flow curve, Eq. (12). The exact criterion for validity can be expressed in terms of viscosity (Barnes et al. 1989) or it can be given in terms of shear rate. In the latter case, it is only valid above some limiting shear rate given by $kD_L{}^m >> 1$.

In practical terms, if we take $kD_L{}^m = 10$, and use the parameters assumed in the earlier section Slope of the equilibrium flow curve, $D_L = 590$, 59 and 0.59 s^{-1} for $\eta_o = 0.3$, 5 and 2000 Pa.s, respectively. The larger η_o is compared with η_∞, the lower the limiting shear rate is in absolute terms. In practice, fitting the Sisko flow curve as an asymptote provides no information on η_o and D_L would be unknown. However, a conservative estimate of η_o can still be made using the viscosity measured at the lowest shear rate.

The Sisko flow curve can be considered in its own right as being valid over the entire shear rate range down to zero. The interesting question is: How is it then related to the Cross model? The rate equation (Eq. 11B) of the Cross model can be generalised by introducing a constant x:

$$\frac{d\lambda}{dt} = a(1 - x\lambda) - b\lambda D^m \tag{34}$$

The EFC is then given by

$$\eta_e = \eta_\infty + \frac{c}{x + kD^m} \tag{35}$$

When $x = 0$, the Sisko flow curve is obtained with $\kappa = c/k$.

The constitutive equations (Eqs. 11A and 34) define a new class of thixotropic fluids of which the Cross and Sisko are special cases. An additional parameter x is introduced which relates to the mechanism of thixotropic recovery. In the case of the Sisko model, $x = 0$ means that the recovery rate is independent of current structure and shear rate. A fluid obeying the Sisko flow curve therefore implies this recovery behaviour.

Conclusion

This paper resolves the discrepancy between the conclusion arrived at in a previous paper (Cheng and Evans 1965), that the equilibrium flow curve (EFC) has positive slope, with experimental data and model predictions that the slope can sometimes be negative. This is undertaken from a phenomenological viewpoint. It is shown that the negative slope is related to the possibility that $(\partial F/\partial\lambda)_e$ along the EFC can be positive as well as negative, and is ultimately traced to the possibility that $(\partial f/\partial\lambda)_e$ is positive for the rate equation. The details are illustrated using the Cross model.

The structural behaviour in the vicinity of an EFC showing negative slope is described and the implication for viscometric measurement is discussed. It is shown that the negatively sloped portion of the EFC can be accessed in *ideal* rheometers under constant shear rate testing, but not under constant shear stress testing. Thixotropic measurements are not often carried out in controlled-stress rheometers. It would be interesting to do so. It is further shown that in wide-gap rheometers and tube, in which the shear stress and shear rate are not uniform, the negatively sloped portion of the flow curve is not accessible under both constant shear stress and constant shear rate testing. Instead, the shear banding phenomenon is obtained, in which the sample in the viscometric gap falls into two distinct bands having different structures and flowing with greatly differing low and high shear rates. This phenomenon is well-known in recent literature and is found in a wide variety of materials, actual as well as theoretical models, which are referenced. The mechanism for the shear banding varies from material to material. The phenomenological description of

thixotropy discussed in this paper constitutes an additional 'mechanism'.

Some literature data of shear stress that decreases with increasing shear rate have been fitted to the Sisko flow curve. The Sisko can be considered the high shear rate asymptote of the Cross flow curve, in which case it is valid only at high shear rates. The implication of the Sisko being valid in its own right and being usable for low shear rates down to zero is investigated. It is seen that the rate equation in the Cross thixotropic model has to be modified according to Eq. (34) and the Sisko flow curve is obtained if the new parameter x is zero. This implies that for the Sisko model, the rate of recovery is independent of structure. Allowing x to be an additional parameter creates a new class of thixotropic model which generalises the Cross model further.

Acknowledgement Thanks to Dr C F Chan Man Fong for helpful comments on this paper.

References

Anand L, Gu C (2000) Granular materials: constitutive equations and strain localization. J Mech Phys Solids 48:1701–1733

Bair S, Winer WO (2000) A study of mechanical shear banding in liquids at high-pressure. Proc XIIIth ICR, Cambridge, UK, pp 3-191–3-193

Barnes HA, Hutton JF, Walters K (1989) An introduction to rheology. Elsevier, Amsterdam

Bautista F, Soltero J, Perez Lopez J, Puig J, Manero O (2000) On the shear banding flow of elongated micellar solutions. J Non-Newtonian Fluid Mech 94:57–66

Britton M, Mair R, Lambert R, Callaghan PT (1999) Transition to shear banding in pipe and Couette flow of wormlike micellar solutions. J Rheol 43:897–909

Chen L, Batra R (1999) The asymptotic structure of a shear band in model-II deformations. Int J Eng Sci 37:895–919

Cheng DC-H (1980) Rheological research project Rep No 14, April-July 1980—Part 3. Comparison of commercial viscometers. Report 3.12A Coaxial cylinder viscometry—Theory and theoretical principles. WSL Rep No CR2037(MH). Warren Spring Laboratory, Stevenage

Cheng DC-H, Evans F (1965) Phenomenological characterization of the rheological behaviour of inelastic reversible thixotropic and antithixotropic fluids. Brit J Appl Phys 16:1599–1617

Cross MM (1965) Rheology of non-Newtonian fluids: a new flow equation for pseudoplastic systems. J Colloid Sci 20:417–437

Decruppe J-P, Lerouge S, Berret J-F (2000) Transient flow birefringence of a viscoelastic solution in shear banding flow. Proc XIIIth ICR, Cambridge, UK, pp 3-342–3-344

Eiser F, Moling F, Porte G, Pithon X (2000) Flow in micellar cubic crystals. Rheol Acta 39:201–208

Ferreiro V, Pennec Y, Seguela R, Coulon G (2000) Shear banding in polyamide 6 films as revealed by atomic force microscopy. Polymer 41:1561–1569

Goveas J, Fredrickson G (1999) Curvature-driven shear banding in polymer melts. J Rheol 43:1261–1277

Kim H, Im S (2000) Approximate analysis of a shear band in a thermoviscoplastic material. J Appl Mech Trans ASME 67:687–694

Kirkwood DH (1994) Semisolid metal processing. Int Mater Rev 39:173–189

Knight JB (1997) External boundaries and internal shear bands in granular convection. Phys Rev 55:6016–6023

Kumar S, Larson R (2000) Shear banding and secondary flow in viscoelastic fluids between cone and plate. J Non-Newtonian Fluid Mech 95:295–314

Lee JY, Magda JJ, Larson RG (2000) Changes in the rheology of a wormy micelle solution due to a twenty-fold increase in concentration. Proc XIIIth ICR, Cambridge, UK, pp 3-208–3-209

Lerouge S, Decruppe JP, Humbert C (1998) Shear banding in a micellar solution under transient flow. Phys Rev Lett 81:5457–5460

Lu C, Olmstead P, Ball R (2000) Effect of nonlocal stress on the determination of shear banding flow. Phys Rev Lett 84:642–645

Lu X, Zhang J, Yang Z (2000) The evolution of shear band of saturated soil. Int J Non-Linear Mech 35:21–26

McLelland ARA, Henderson NG, Atkinson HV, Kirkwood DH (1997) Anomalous rheological behaviour of semi-solid alloy slurries at low shear rates. Mater Sci Eng A 232:110–118

Oda M, Kazama H (1998) Microstructure of shear bands and its relation to the mechanisms of dilatancy and failure of dense granular soils. Geotechnique 48:465–481

Olmsted PD, Radulescu O, Lu C-YD (2000) Shear banding in the diffusive Johnson-Segalman model. Proc XIIIth ICR, Cambridge, UK, pp3-228–3-230

Radulescu O, Olmsted P, Lu C (1999) Shear banding in reactive-diffusive models. Rheol Acta 38:606–613

Radulescu O, Olmstead PD, Berret J, Porte G, Lerouge S, Decruppe J-P (2000) Kinetic aspects of shear banding in surfactant systems. Proc XIIIth ICR, Cambridge, UK, pp3-336–3-362

Remmelgas J, Leal G (2000) Numerical studies of viscoelastic flows using a model for entangled polymer solutions with a shear stress maximum. J Non-Newtonian Fluid Mech 90:187–216

Sisko AW (1958) The flow of lubricating greases. Ind Eng Chem 50:1789–1792

Tanaka H (2000) A simple phenomenological model of shear banding in a polymeric fluid with a non-monotonic constitutive law. Proc XIIIth ICR, Cambridge, UK, pp 3-182–3-184

Volkova O, Cutillas S, Bossis G (1999) Shear banded flows and nematic-to-isotropic transition in ER and MR fluids. Phys Rev Lett 82:233–236

Whorlow RW (1992) Rheological techniques. Ellis Horwood, Chichester